

Article

Contribution of ERT on the Study of Ag-Pb-Zn, Fluorite, and Barite Deposits in Northeast Mexico

José Alberto Batista-Rodríguez ^{1,*}  and Marco Antonio Pérez-Flores ²¹ Escuela Superior de Ingeniería, Universidad Autónoma de Coahuila, Nueva Rosita, Coahuila 26800, Mexico² División de Ciencias de la Tierra, CICESE, Baja California 22860, Mexico; mperez@cicese.mx

* Correspondence: josebatista@uadec.edu.mx

Abstract: The results on the effectiveness of five 2D electrical resistivity tomography (ERT) survey profiles for Ag-Pb-Zn, fluorite, and barite exploration Mississippi Valley Type (MVT) and on the magmatic deposits of northeast Mexico, are presented. The profiles were made in areas with mining activities or mineralization outcrops. Schlumberger, dipole-dipole, and Wenner array configurations were used on the measurements. The results showed that electric resistivity can be used to distinguish between mineralized zones. In magmatic-type Pb-Zn and MVT Pb-Zn deposits, resistivity values are shown as low. In magmatic-type fluorite and MVT fluorite deposits, as well as the MVT barite deposit, low-resistivity values are related to Fe sulfides and clays. With these results it is possible to connect observed surface mineralization with underground mineralization. New mineralized zones are also found and their geometries, extensions, and dipping are reported. Therefore, lower resistivity values can be linked to mineral bodies with higher Ag-Pb-Zn contents, as well as bodies enriched in Fe sulfides, Fe oxides, and clays in the fluorite and barite mineralizations. In most ERT models, fractures and faults are identified, indicating a structural control on mineralization. From the geoelectric patterns we can infer the magmatic and MVT origin of these mineral deposits.

Keywords: electrical resistivity tomography; mineral exploration; MVT deposit; magmatic deposit; northeastern Mexico



Citation: Batista-Rodríguez, J.A.; Pérez-Flores, M.A. Contribution of ERT on the Study of Ag-Pb-Zn, Fluorite, and Barite Deposits in Northeast Mexico. *Minerals* **2021**, *11*, 249. <https://doi.org/10.3390/min11030249>

Academic Editors: Mario Zarroca, Roberto Rodríguez and Isaac Corral

Received: 24 December 2020

Accepted: 24 February 2021

Published: 27 February 2021

Publisher's Note: MDPI stays neutral with regard to jurisdictional claims in published maps and institutional affiliations.



Copyright: © 2021 by the authors. Licensee MDPI, Basel, Switzerland. This article is an open access article distributed under the terms and conditions of the Creative Commons Attribution (CC BY) license (<https://creativecommons.org/licenses/by/4.0/>).

1. Introduction

Mexico is an important producer of silver, celestine, fluorite, lead, zinc, barite, antimony, manganese, and gold [1]. Fluorite, barite, celestine, and Pb-Zn deposits occur in northeastern Mexico, within Mesozoic carbonates [2]. These deposits belong to a wide variety of ore deposit types, such as epithermal, skarn and MVT [3]. There are over 200 MVT Zn-Pb and associated celestine, fluorite, and barite deposits in the state of Coahuila and neighboring areas in northeastern Mexico. These deposits define a metallogenic province, named the MVT province of northeastern Mexico [2,4].

Geophysical methods are widely used in mineral exploration because mineral deposits have physical properties that contrast with their host rocks [5–11]. Electrical resistivity is a physical property that generally shows a contrast between mineralized units and host rocks [5–7]. Particularly, electrical resistivity tomography (ERT) is used to detect and characterize MVT and magmatic deposits [5,7,8]. ERT models with resistivity values between 300 and 500 Ωm [9] and from 730 to 1500 Ωm [10] have been obtained in some barite deposits. In Pb-Zn mineral deposits a low-resistivity anomaly is observed which is related to sulfide mineralization [5,7,11].

Some characteristics of the MVT and magmatic deposits, are their location in carbonate rocks, their sulfides, barite, and fluorite epigenetic mineralization (originated at shallow depth) [12,13], which suggest that geophysical methods, particularly ERT, can provide good results on the location and characterization of these deposits.

The aim of this study is to show the preliminary contribution of electrical resistivity tomography to locate and characterize Ag-Pb-Zn, fluorite, and barite MVT and magmatic deposits in northeast Mexico (Figure 1).

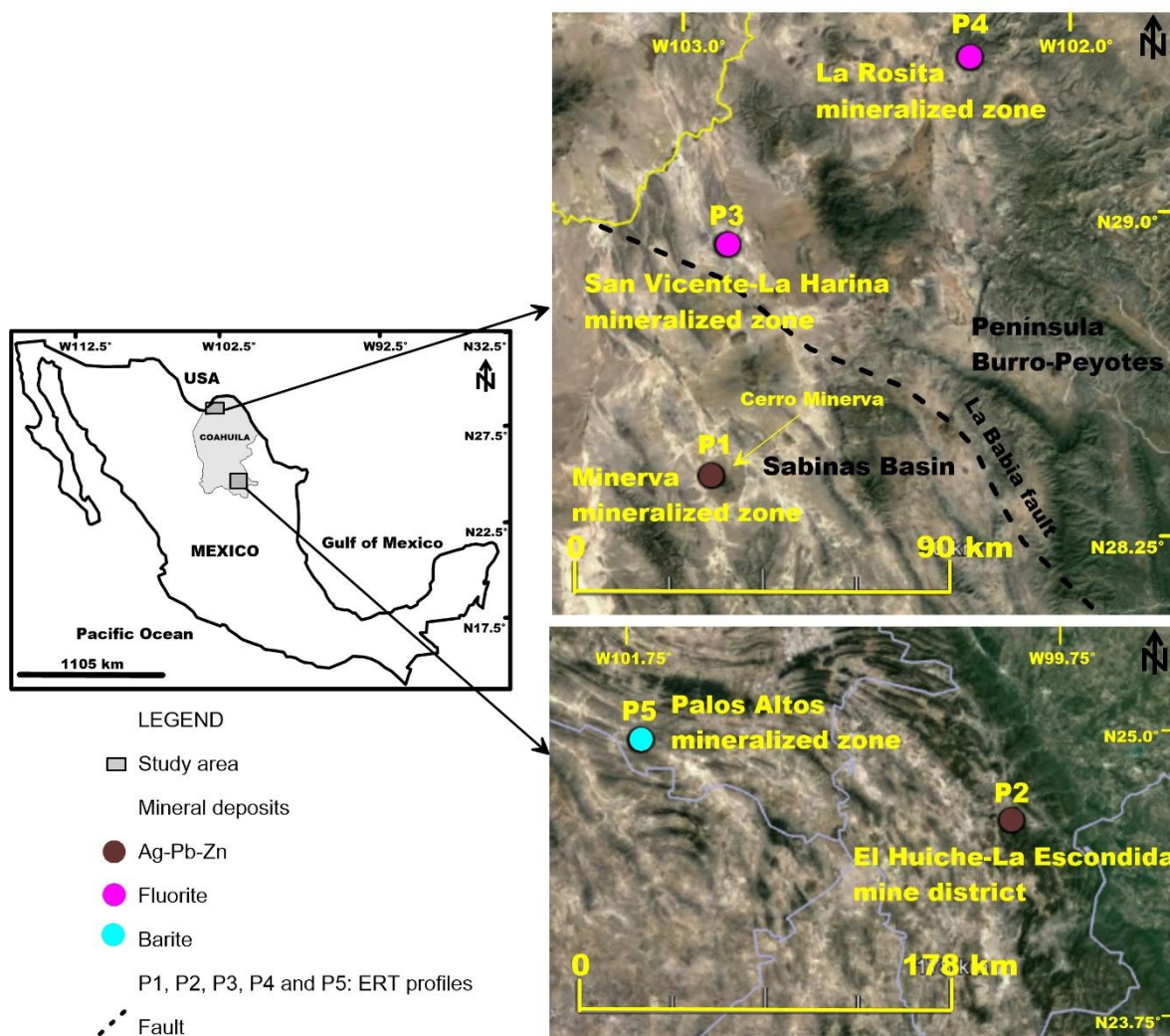


Figure 1. Location of the study area in northeast Mexico (Coahuila state). Profiles P1 and P4 are in magmatic deposits. Profiles P2, P3, and P5 are in MVT deposits. P1 is in the Minerva Mine, P2 in Guadalupe Mine, P3 in El Otomí mine, P4 in Juan Valencia mine, and P5 in El Tapón mine.

2. Geological Setting

Mineral deposits in Coahuila are dominated by MVT-like fluorite deposits. This region also has significant magmatic-hydrothermal deposits associated with the East Mexican Alkaline Province, which correspond mostly to skarn type [14]. In this region, fluorite, barite, celestine, and MVT Pb-Zn deposits are found. These deposits are located inside the MVT metallogenic province of northeastern Mexico in different Mesozoic sedimentary formations of the Sabinas Basin, linked to the beginning of the Laramide Orogeny [2]. These ore deposits occur in Mesozoic carbonate rocks, partially deformed by Laramide tectonics [2,13].

The Ag-Pb-Zn deposits in northern Mexico are hosted in thick carbonate-dominated Jurassic-Cretaceous sedimentary sequences. These mineral deposits contain irregular ore bodies that commonly reveal strong structural controls. The deposits are generally controlled by a combination of folds, faults, fractures, fissures, and intrusive contact that acted as structural conduits for channeling mineralizing fluids to favorable sites of deposition. These deposits show three principal morphological types: mantos, chimneys,

and pods and are composed of massive sulfides and/or calc-silicate skarn. Sulfide mantos and chimneys are enclosed within carbonate rocks [15].

Zn-Pb deposits are made up essentially of sulfides and generally exhibit supergene alteration with the consequent alteration of sulfides to oxides, carbonates, and sulfates [2]. Most of these deposits have been described in the Cupidito, Cupido, La Virgen, Aurora, and Acatita Formations [2,13], as well as in the Olvido and Santa Elena Formations [16,17].

In the Cupidito Formation (early Aptian) the smaller Pb-Zn bodies appear as strata-bound mantos which are concordant with the stratigraphy, while the larger bodies are found filling paleokarst. When sulfides are oxidized, the host rocks adopt reddish and yellowish tones. At the base of the Georgetown Formation (late Albian), there is small sub-economic mineralization of Pb-Zn sulfides. The mineralization is filling in small karst structures and fractures with different thicknesses. Generally, the primary mineralization is oxidized [2].

Three types of clearly epigenetic fluorite deposits are reported in northeastern Mexico within carbonate rocks [13]: the first is MVT, in which the fluorite mantos are related to compressive structures, and which shows no relationship with the intrusive rocks; the second type is related to magmatic processes, and; the third type includes small fluorite bodies in skarn-type deposits developed around post-Laramide rhyolitic bodies.

Along the edge of the Burro-Peyotes Paleopeninsula (Figure 1), a high concentration of strata-bound fluorite bodies is found within the Washita Group [2]. In the La Encantada-Buena Vista fluorite district (located east of the Minerva mineralized zone; Figure 1), the fluorite bodies exhibit strong structural controls and contain clay minerals [13]. The Aguachile district (located west of the Rosita mineralized zone; Figure 1) and neighboring areas contain a variety of fluorite deposits. At the Aguachile deposit, the fluorite bodies have a magmatic relationship with tertiary rhyolites. This deposit comprises a ring dyke hosted in Mesozoic limestone that developed Fluorite-Be mineralization around the dyke. This fluorite mineralization also contains hematite, iron oxyhydroxides, and illite [3].

In the study region, fluorite deposits are reported in several geological carbonate formations, mainly the Georgetown, Salmon Pick, Santa Elena, and Del Río Formations [2]. The barite deposits have been reported in the Olvido, La Virgen, Cupidito, and Cupido Formations [2,13], as well as in the Zuloaga Formation [18]. The La Virgen Formation of Early Cretaceous age (Barremian) is made up of gypsum and limestone. The barite bodies are also stratiform, exhibiting strong fracturing, and were infilled with Pb-Zn sulfides during the supergene oxidation process [2].

2.1. Studies Zones of Mineralization

2.1.1. Minerva Mineralized Zone

This zone mainly contains metallic Ag-Pb-Zn mineralization of magmatic origin, restricted to the peripheral part of Cerro Minerva. The mineralization consists of a lenticular manto whose origin is related to contact metasomatic processes (skarn) between the intrusive bodies and limestones of the Santa Elena Formation of Early Cretaceous age (Late Albian). This mineralization has preferential Ag-Pb-Zn values, in a mixture of sulfides, iron oxides, and clays [16].

At the Minerva mine (P1 in Figure 1), the Santa Elena Formation is made up of dark gray limestone with a mudstone and wackestone texture. This formation has a lenticular manto with values of Ag (99 g/t), Pb (2.18%), and Zn (11.51%), with a direction N 45° W and a dip from 35° to 65° NE. Its mineralogy consists of a mixture of sulfides and oxides, such as argentite, galena, sphalerite, chalcopyrite, and magnetite, within an iron oxide matrix with calcite associations, gypsum, and clays [16].

2.1.2. El Huiche-La Escondida Mine District

In this mining district, Ag-Pb-Zn mineralization occurs within breccias with iron oxides and clays. Such mineralizations have been reported in gypsum and limestone lenses of the Olvido Formation of Late Jurassic (Oxfordian-Kimmeridgian). In the Guadalupe

mine (P2 in Figure 1), this mineralization is of MVT-type and has iron oxides, manganese, and disseminated pyrite, with traces of Ag and average values of 0.008 g/t Au, 0.095% Cu, 0.682% Pb, 1.81% Zn, and 0.28% Mn [17].

2.1.3. San Vicente-La Harina Mineralized Zone

In this zone, fluorite mineralization is mainly reported in the Santa Elena Formation of Early Cretaceous (Late Albian), which is composed of dark gray limestones with a mudstone to wackestone texture. The fluorite occurs in veins with a lenticular behavior, erratic in their direction and depth, and their thickness varies from 0.10 to 1.20 m. All reported mining prospects have small mining works that had reached up to 35 m in depth. Generally, there is 20% to 30% CaF₂, although some mines have more than 60% CaF₂. In this mineralized zone, the El Otomí mine (P3 in Figure 1) has MVT fluorite associated with iron oxides and clays [19].

2.1.4. La Rosita Mineralized Zone

This mineralized zone contains fluorite bodies within the Salmon Pick Formation of Early Cretaceous (Middle-Late Albian) age. This formation is composed of gray dolomitic wackestone and grainstone with abundant flint nodules in a dolomitized limestone, with dolomites occurring at its base. In the Juan Valencia mine (P4 in Figure 1), this formation contains fluorite bodies of magmatic origin. The mineralization appears in a vein with a 120 m length, and a N 50° E direction and a 65° SE dip. Along with fluorite, iron oxides (such as hematite, goethite, and limonite) and clays are reported filling fault areas that control mineralization. Fluorite sometimes fills fractures related to this fault. Generally, the CaF₂ contents vary from 1.03% to 30.2%, although 74.45% CaF₂ has been reported in one sample [20].

2.1.5. Palos Altos Mineralized Zone

In this zone, MVT barite mineralization is reported within the limestone of the Zuloaga Formation of Late Jurassic (Oxfordian-Kimmeridgian). The barite bodies are stratiform in the form of irregulars manto with iron oxides and clays resulting from the oxidation of Pb-Zn sulfides. In this formation, values from 3.11% to 77.25% BaSO₄ have been detected. At the El Tapón mine (P5 in Figure 1), a mineralized breccia has been observed and the limestone layer has been recorded to dip to the south with a 19° angle [18].

All mineralized zones studied are located within the MVT Province of Northeast Mexico proposed by González-Sánchez et al. [4]. Within this province, mineral deposits of barite, fluorite, and Ag-Pb-Zn are reported, accompanied by iron oxides and clays originated from the sulfide oxidation [2,3,20]. The iron sulfides and clays are good conductors for ERT and therefore, must display contrasting values in resistivity compared with the sedimentary host rocks [7]. This helps detect and delimit the mineral bodies. The Ag-Pb-Zn deposit in the Minerva zone [16] and fluorite deposit in the La Rosita zone [20], are the only ones that show an evident relationship with igneous rock bodies. In the other three mineralized zones, the mineralization shows strata-bound characteristics.

3. Materials and Methods

Electrical resistivity tomography (ERT) data were acquired through five profiles (P1, P2, P3, P4, and P5 in Figure 1) using an AGI SuperSting R1/IP/SP (Austin, TX, USA) (Figure 2) [21]. IP and ERT methods are commonly used to locate mineral deposits, however, it was decided to use only ERT because the research aimed at showing the preliminary contribution of ERT in the mineral exploration in the region. Furthermore, the measured resistivity values reasonably delimited the mineral bodies observed on the surface and in the mining works. Schlumberger, dipole-dipole, and Wenner array configurations with 28 electrodes spaced every 20 m were used. This electrode spacing was used to cover most of the mineral deposits and to assess the preliminary contribution of electrical resistivity tomography to locate and characterize mineral bodies. Since only preliminary results were

aimed at and because obtained resistivity models reasonably delimited the mineral bodies observed on the surface and in the mining works, we discarded using smaller electrode spacing. However, the use of smaller electrode spacings might be necessary for more accurate characterization of the geometry of imaged mineral bodies. The profiles reach an approximate length of 540 m. With the extension of 540 m begin possible to reached up to 130 m, however, our study areas were mainly composed of highly resistive limestone, therefore, we discarded the deepest data because of their low signal-to-noise ratio. Only one profile was measured in each mineral deposit to preliminary assess the contribution of ERT in the characterization of the minerals bodies.



Figure 2. Data collection using the AGI SuperSting R1/IP/SP. (a) SuperSting™ console, (b) Switch box, (c) Battery, (d) Electrode.

This kind of eq highly resistive limestone, therefore, we uipment has automated switching that makes the work faster. We first ground the electrodes. Then we could easily measure Schlumberger, Wenner and dipole-dipole arrays according to a previous deployment design. Some authors discuss the advantages of every array over the others with synthetic data and their results may be contradictory [22,23]. Without entering into such a discussion, we merged the three data sets (dipole-dipole, Schlumberger and Wenner arrays) in a single entrance file in order to get a single resistivity model from the inversion process. The root mean square (RMS) reported is the one obtained when using the merged three data sets. We assumed that the more information used for the inversion process the better model obtained, but we also assumed that every array had a different electrical current pattern in the ground, and therefore, every array imaged the ground in a slightly different way. The use of the three different current patterns from the three arrays gave us a more accurate image of the ground resistivity [24]. EarthImager 2D from the AGI company was the program used for the inversion process. This program is getting a standard in industry. It solves the resistivity inversion by means of finite elements modeling. An L_2 norm method was used for the inversion process. As an initial model, we assumed a homogeneous half-space with a resistivity that was the average of all the resistivity measurements in each profile. A representative resistivity value is taken from the variance recorded along the acquisition process of each measurement. The final resistivity model obtained was considered the best fitted model, and the model residuals were determined as the RMS.

The 2D ERT survey was carried out in five mineralization zones, in which the mineralization was partly noticed on the ground surface or through mine activity. The first and second zones (profiles 1 and 2; P1 and P2 in Figure 1) contained Ag-Pb-Zn mineral deposits of magmatic and MVT type, respectively. In the third and fourth zones (profiles 3 and 4; P3 and P4 in Figure 1) there were fluorite mineral deposits of magmatic and MVT type, respectively. The fifth zone (Profile 5; P1 in Figure 1) hosted a barite mineral deposit considered MVT-type. All profiles were oriented perpendicular to the direction of the mineralizations and the dip of rock sequences.

The measurements acquired in the field were processed using the commercial software EarthImager2D [25]. The inversion process was based on the finite element algorithm to compute the true resistivity with the apparent resistivity data. The software allowed us to do a single inversion of every array or the use of the three arrays for getting a single resistivity model. The number of iterations varied from five to eight with the root mean square (RMS) reaching 3.34 to 7.66%.

In each ERT, we showed the kind of rock that outcrops, as well as the outcrops of mineral bodies and old mining works, in order to facilitate interpretation. These outcrops of mineral bodies, as well as vertical well and underground galleries of old mining works, were used for the reduction of ambiguity in the interpretation. We assumed that the mineralized zones were low resistivity bodies delimited by high resistivity due to carbonated sedimentary rocks. Therefore, we assumed that the decrease in the resistivity values was the effect of higher mineralization concentrations and/or alteration minerals because of the direct relationship between the mineralizations on surface and mining works with relatively low resistivity values. In Ag-Pb-Zn deposits, mineralization in a mixture of iron sulfides, iron oxides, and clays could be found [16,17], accordingly, mineralization and clays cause the decrease in resistivity values. In fluorite and barite deposits, the mineralization was associated with iron oxides and clays originated from iron sulfide alteration [18–20]. This mineral association indicated that the decrease in the resistivity values is mainly related to these alteration minerals.

4. Results

In the studied profiles, outcropping sedimentary rocks were represented mainly by Jurassic and Cretaceous limestone. The profiles had N-S, NE-SW, and NW-SE directions, and mineralization outcrops, leading to the observed mining activities. Electrical resistivity models were obtained in these mineralized zones. These were helpful for continuing to explore the surface mineralization to depths, but also to identify new underground mineralized bodies with no surface connection.

The models showed resistivity values ranging between 1 and 100,000 Ωm , and mineralized zones located in zones of low resistivity delimited by high resistivity. In some ERT models, the sedimentary sequences and the layers dip were well delimited. Similarly, the low-resistivity values helped identify fractures and faults. Some of these structures controlled the characteristics of the mineralized zones. Below are the details about the interpretation of the inverted ERTs or resistivity models.

4.1. Ag-Pb-Zn Deposits

Profiles 1 and 2 were located in Ag-Pb-Zn polymetallic deposits. Profile 1 occurred in an Ag-Pb-Zn deposit of magmatic origin which belonged to the Minerva mineralized zone, in which the mine with the same name was studied (P1 in Figure 1). Ag-Pb-Zn mineralization in a mixture of iron sulfides, iron oxides, and clays could be found in this mine [16]. Iron sulfides and clays are good conductors and could therefore help detect the associated Ag-Pb-Zn mineral bodies in this deposit [7].

Limestone outcrops of the Santa Elena Formation of Early Cretaceous, Albian were found in profile 1 (Figure 3a). There were also caliche outcrops in two small areas ($X = 0\text{--}60\text{ m}$ and $X = 80\text{--}160\text{ m}$), as well as Ag-Pb-Zn mineralization outcrops ($X = 60\text{--}80\text{ m}$)

at the SE end of the profile. A vertical well of old mining work with a depth of 12 m was located at the center of the profile ($X = 245$ m) (Figure 3b).

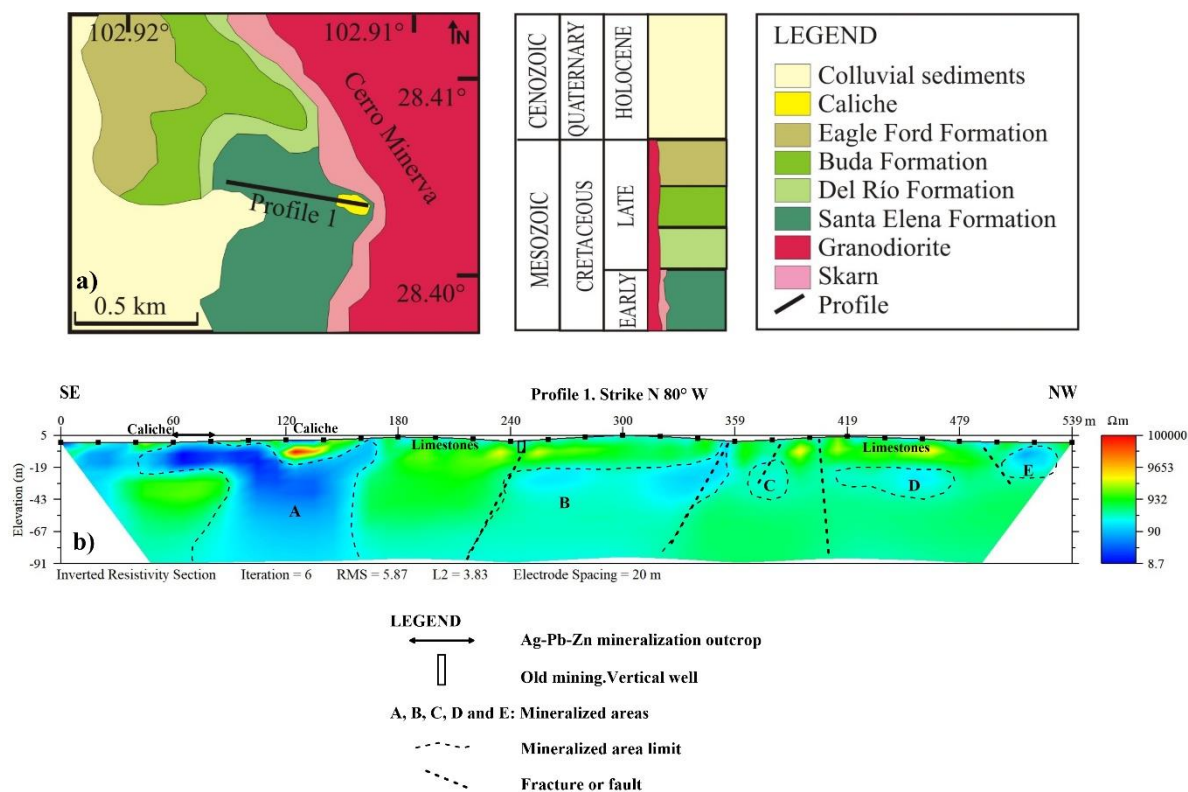


Figure 3. (a) Geological map of the Minerva mine. Modified from Herrera-Monreal and Rodríguez-Rodríguez [16]. (b) Inverted resistivity section or resistivity model. ERT in a magmatic-type Ag-Pb-Zn deposit. The stratigraphic column is not to scale.

The ERT model of the resistivity showed a range between 8.7 and 100,000 Ωm with a RMS of 5.87%. The mineralization shown on the surface and in the vertical well occurred in areas with low resistivity values (lower than 510 Ωm), delimited by high resistivity values. The resistivity values of the Ag-Pb-Zn sulfide mineralization were contrasting with those of the host limestone. The low resistivity was used to identify and delineate this mineralization in the subsurface. The outcropping mineralization was identified as zona A (Figure 3b), in which, the resistivity ranged between 8.7 and 510 Ωm . This zone had a length between 60 and 80 m, with a depth exceeding 90 m. It was very shallow in places (approximately 5 m depth) but did not outcrop. Using the low resistivity values (lowest than 510 Ωm), other mineralized zones could be identified within the limestone (B, C, D, and E in Figure 3b), and many of them were related to fractures or faults. The mineralization, around the vertical well appears to be related to a fracture or fault that extended more than 90 m at depth.

The mineralized zone B had resistivity values between 90 and 510 Ωm , extended more than 120 m in length, and was laterally limited by fractures or faults. This zone had more than a 20 m depth, except for its lateral limits, where fractures or faults allowed mineralization, and the zone could be shallower. Zones C, D, and E were smaller than the two previously described zones (A and B). These were located at more than 20 m depths, except for zone E, which had an approximately 10 m depth. Zones C and D had resistivity values from 300 to 510 Ωm , while zone E had resistivity values from 80 to 510 Ωm .

Profile 2 was taken in an MVT Ag-Pb-Zn deposit of the El Huiche-La Escondida mining district. In this district, the Guadalupe mine (P2 in Figure 1) was studied, in which limestone from the Olvido Formation outcrops (Figure 4a). In this rock, the Ag-Pb-Zn

mineralization appeared in iron oxides and clays, originated from the sulfide alteration [17]. Such minerals are good conductors and showed contrasting resistivity with the sedimentary host limestone [7].

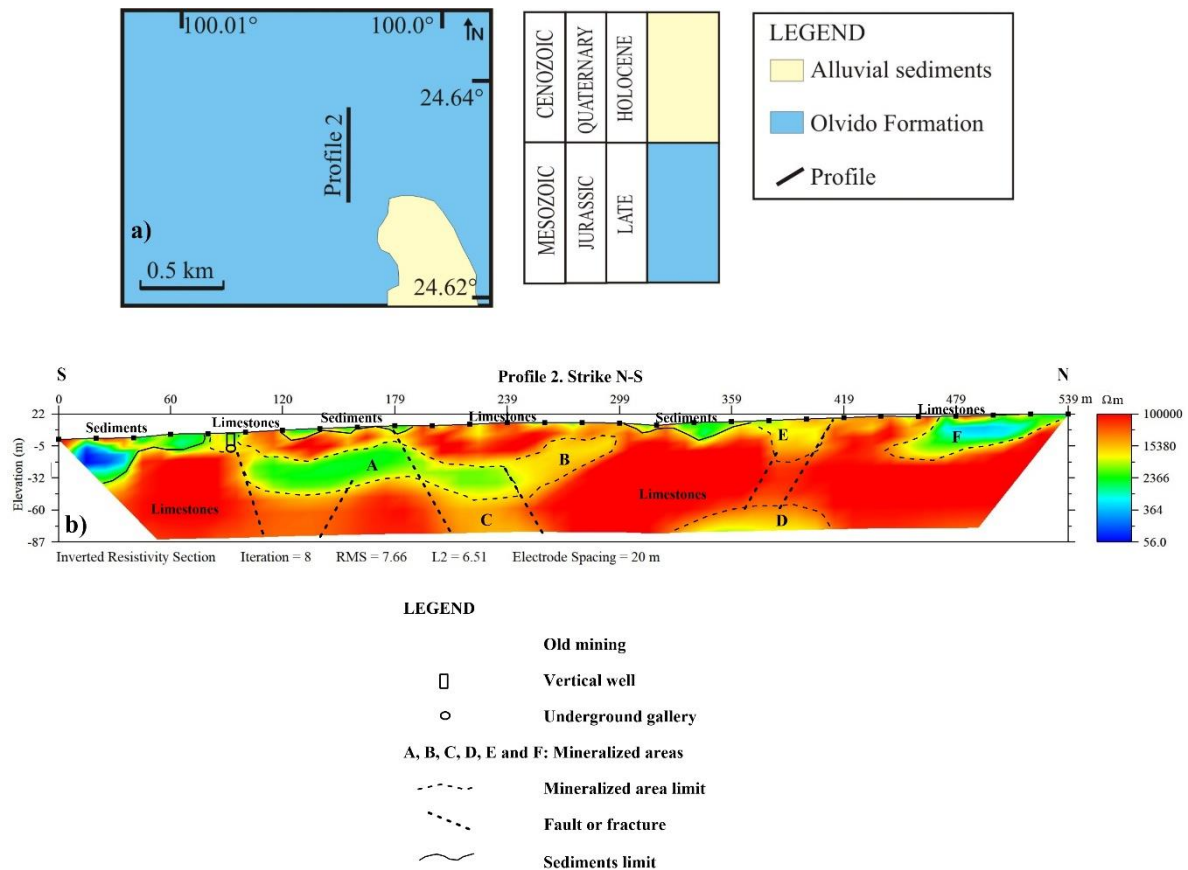


Figure 4. (a) Geological map of the Guadalupe mine. Modified from Montañez-Castro [17]. (b) Inverted resistivity section. ERT in MVT Ag-Pb-Zn deposit. The stratigraphic column is not to scale.

In this profile, sediments and limestone outcrop (Figure 4a) where some old mining works (a vertical well with a depth of 10 m and underground galleries) were developed, and high Ag-Pb-Zn contents were extracted (Figures 4b and 5). The vertical well reaches an underground gallery at a depth of 10 m. The ERT model showed a variation range between 56 and 100,000 Ωm with a RMS of 7.66% (Figure 4b). Low resistivity values (lower 8000 Ωm) delimited by high resistivity were obtained in areas of metallic mineralization (according to the mine information in the vertical well and underground galleries). This zone extended northward, being more than 160 m length, with an approximate 25 m thickness and a maximum depth of 55 m (A in Figure 4b). This zone also had variable dips, apparently related to faults.

The relationship between the mining work (vertical well and underground galleries) that cuts the mineralization and the resistivity values allowed other mineralized zones to be located (B, C, D, E, and F in Figure 4b). In the mineralized zones A and F, the resistivity was lower. In zone A, the resistivity decreased to 1.300 Ωm , and in zone F, it decreased to 200 Ωm . This last zone was shallower (less than 10 m deep) and was located at the north end of the profile. This zone reached more than 80 m in length, dipping southward, and reached 40 m depths. Mineralized zone B may be a continuation from the north end of the mineralized zone A, delimited by a fault. This zone B dipped southward and had a depth between 10 and 50 m. Mineralized zone C could also be a continuation of zone A at a depth greater than 80 m. Zone C was sub-vertical and appeared to be delimited laterally

by a fault. The mineralized zones D and E were related through faults. Zone D was located 60 m deep and zone E was very shallow.

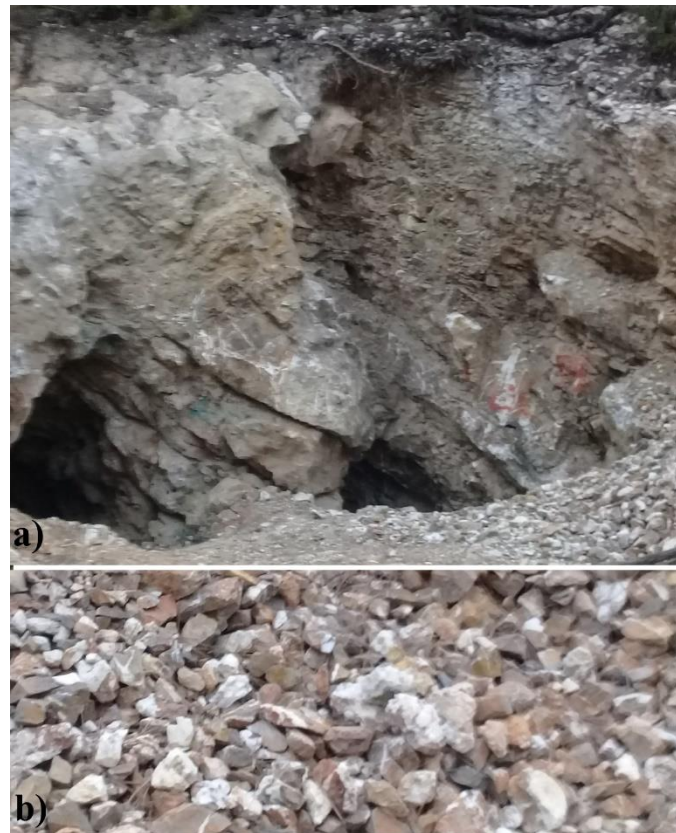


Figure 5. Mine activity in MVT Ag-Pb-Zn deposit. (a) underground galleries. (b) Material extracted from mining. The subfigures do not need a scale bar.

4.2. Fluorite Deposits

Profiles 3 and 4 cross-cut fluorite deposits. Profile 3 was from an MVT fluorite deposit at the Otomí mine within the San Vicente-La Harina mineralized zone (P3 in Figure 1). In this mine, limestone from the Santa Elena Formation of Early Cretaceous (Albian) age outcrops (Figure 6a). At the center of the profile, there was also an area of unconsolidated materials and limestones, which were both highly oxidized and red in color (Figure 7). This zone had iron sulfides whose alteration produced iron oxides and clays. Both mineral groups are good conductors [7] and could help to detect the fluorite bodies in this deposit.

In profile 3, vertical wells showed that fluorite mineralization outcrops were located in old mining works (1, 2, and 3 in Figure 6b). In this deposit, the fluorite mineralization was related to areas enriched in iron oxides and clays. The fluorite mineralization detected in vertical well 2 occurred in a highly oxidized limestone sequence. In vertical wells 1 and 3, the mineralization occurred less oxidized limestone, that is, less enriched in iron oxides and clays. The extent of this area and the unconsolidated materials in the subsurface are indicated in interpreted ERT (Figure 6b).

In the ERT model of profile 3, the resistivity ranged between 10.4 and 100,000 Ωm , with a RMS of 3.34% (Figure 6b). In the fluorite outcrop, and around the vertical wells, resistivity values were less than 5000 Ωm , delimited by larger resistivity values. These low resistivity values allowed the delimitation of the mineralization within the limestone sequence (A, C, E, and F in Figure 6b). New mineralized zones were also revealed with these resistivity values (B, D, G, H and I in Figure 6b). In general, the mineralization reached a depth greater than 85 m.

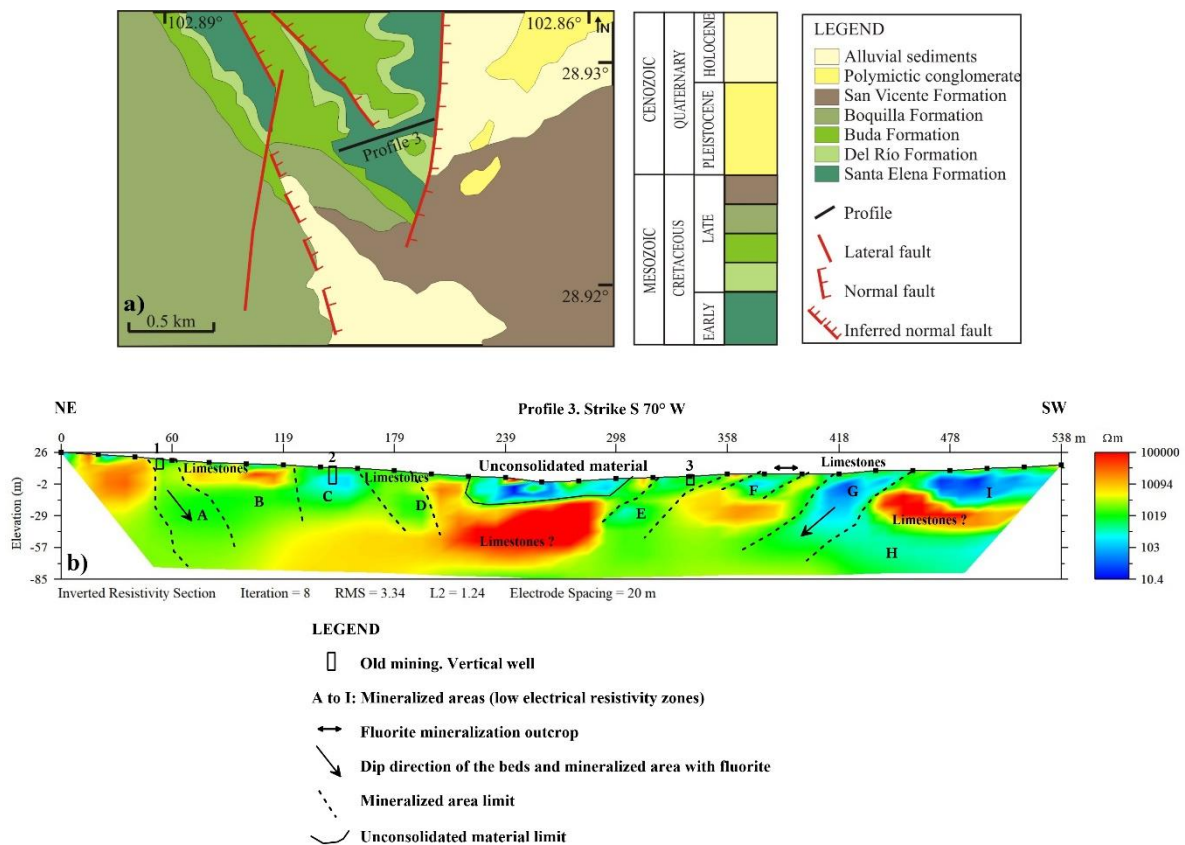


Figure 6. (a) Geological map of the Otomí mine. Modified from Ramírez-Gutiérrez and Chávez-Rangel [19]. (b) Inverted resistivity section. ERT in MVT fluorite deposit. The stratigraphic column is not to scale.



Figure 7. Iron oxide and clays zone in profile 3.

In the interpretation of the ERT model of profile 3, the mineralized zones dipped towards the SW in the first part of the profile. This dip was similar to the dip of the limestone layers described in the mine [19].

The second part of the profile was located in the zone with the lowest topographic height to the profile end. In this second part, the mineralized zones and, therefore, the limestone layers dipped towards the NE. The differences in the dip direction in both parts

of the profile showed its location in a folded area (anticline at both ends and syncline at the profile center; Figure 6b).

Profile 4 occurred in a magmatic-type fluorite deposit. This deposit was hosted in the La Rosita mineralized zone, in which the Juan Valencia mine was studied (P4 in Figure 1). Limestones from the Salmon Peak Formation of Early Cretaceous, Middle-Upper Albian age outcrop in this mine (Figure 8a). Fluorite veins were observed in these rocks, generally controlled by faults with iron oxides and clays originated from iron sulfide alteration [20]. Such minerals are good conductors [7], and therefore, could help detect the associated fluorite bodies in this deposit. An igneous rock dike (rhyolite porphyry) outcropped in the first 20 m of profile 4 (NW end; Figure 8a,b). Otherwise, only very compact limestones were seen. At the NW end, at a 20 m depth, a horizontal gallery of the old mining works was located (Figure 8b).

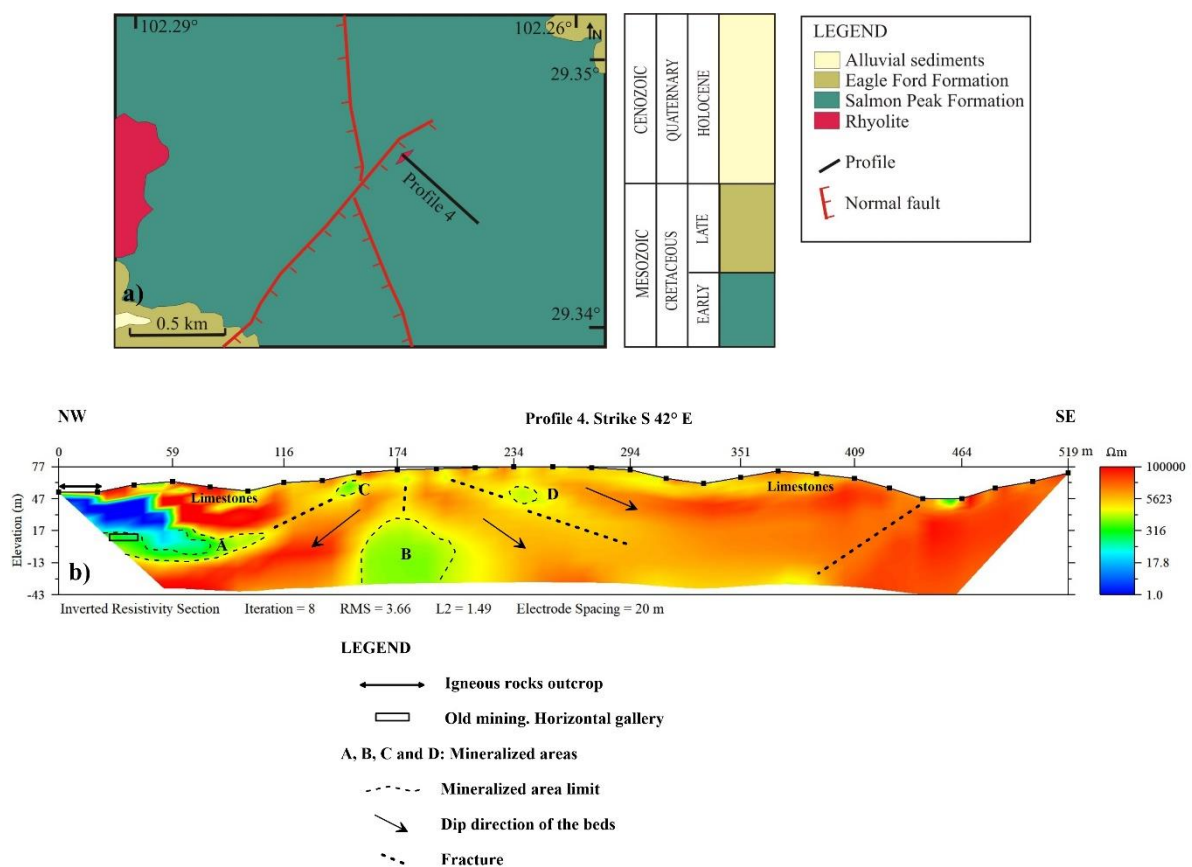


Figure 8. (a) Geological map of the Juan Valencia mine. Modified from Bernales-Azúcar et al. [20]. (b) Inverted resistivity section. ERT in a magmatic-type fluorite deposit. The stratigraphic column is not to scale.

In the ERT model of profile 4, the resistivity ranged from 1.0 to 100,000 Ohm-m, with an RMS of 3.66% (Figure 8b). In this section, high resistivity is predominantly related to compact limestone. Resistivities lower than 180 Ωm occurred in an igneous rocks dike. The zone that included the horizontal gallery was associated with resistivities between 180 and 1600 Ωm. Such resistivity values were related to iron oxides and clays associated with fluorite mineralization. This resistivity range allowed us to continue delimiting the fluorite mineralization within the limestone sequence (A in Figure 8b). Similarly, those resistivity values revealed other mineralized zones (B, C and D in Figure 8b).

All mineralized zones had the same resistivity ranges, indicating similar iron oxides and clay contents in such zones. The mineralized zone A was hosted in the contact area between igneous and sedimentary rocks. This possibly extended SE through a fracture, fault, or stratigraphic contact. The structure dip to the NW related this zone to the shallower

mineralized zone C (lower than 10 m depth). The largest mineralized zone (zone B), started at a 45 m depth and reached more than 90 m of depth with an approximate diameter of 30 m. This zone should be related to a fracture or fault that reached the surface. To the SE of zone B, there was another smaller mineralized zone (zone D), located at a depth of 15 m. This last zone was also related to fractures or faults.

4.3. Barite Deposit

The ERT model in profile 5 was hosted in the MVT-type barite deposit of the El Tapón mine belonging to the Palos Altos mineralized zone (P5 in Figure 1). In the profile, limestones from the Zuloaga Formation of Late Jurassic, Oxfordian-Kimmeridgian age outcrop (Figure 9a). In this rock, barite mineralization was observed in one of the breccia outcrops with iron oxides and clays (Figure 10). A vertical well with a depth of 15 m had been made in this outcrop. This well was developed in past mining activities. The iron oxides and clays originated from the oxidation of Pb-Zn sulfides associated with barite mineralization. Such minerals are good conductors [7] and could help detect the associated barite mineral bodies in the deposit.

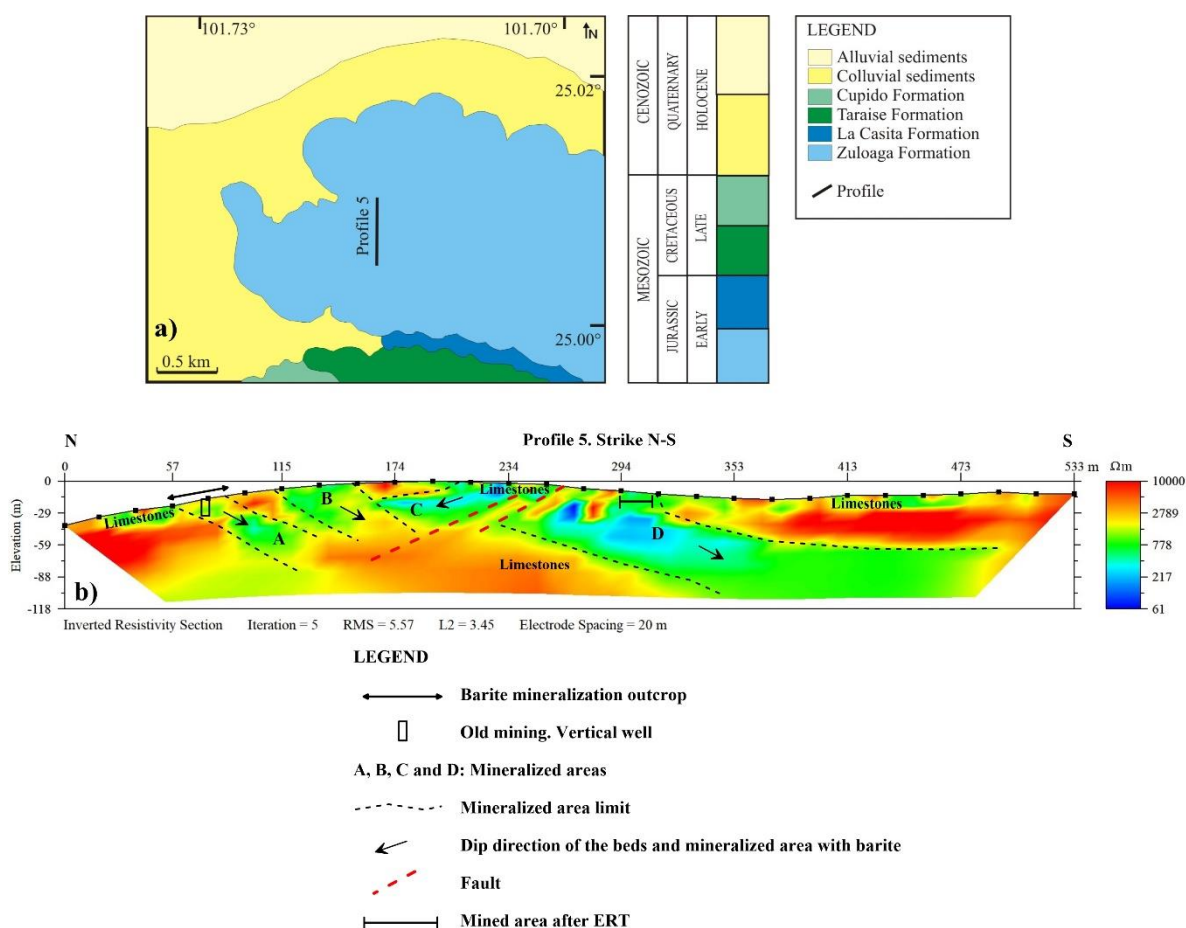


Figure 9. (a) Geological map of the El Tapón mine. Modified from Santiago-Carrasco and Maciel-Hernández [18]. (b) Inverted resistivity section. ERT in the MVT-type barite deposit. The stratigraphic column is not to scale.



Figure 10. Outcrop of barite mineralization within a zone with iron oxides and clays located in profile 5. The red line indicates the possible limit of barite mineralization.

In the ERT model of profile 5, the resistivity ranged from 61 to 10,000 Ωm with an RMS of 5.57% (Figure 9b). In the barite outcrop and around the vertical well, relatively low resistivity values were obtained (lower than 650 Ωm), delimited by high resistivities. This relationship between resistivity values and barite mineralization had allowed the estimation of the extension and location of this mineralization within the limestone sequence (A in Figure 9b). The resistivity data also showed the existence of another mineralized zone with a similar signature (B, C and D in Figure 9b). These zones were relatively shallow and could reach depths greater than 118 m (view zone D in Figure 9b). Most of these mineralized zones were southward dipping, following the general dipping of the rock sequence in the mine [18]. Zone C presented a different overall dip (northward), apparently related to a fault. This structure dipped northward and cut the profile in a NW-SE direction, which was related to the tectonic characteristics of the region [18]. The highest resistivity values were related to compact limestone, that is, limestone which has few fractures [7].

After interpreting the ERT, one mining activity was carried out in zone D and barite mineralization was found at a 19 m depth, within a breccia zone with iron sulfides, iron oxides, and clays.

5. Discussion

In the magmatic-type Ag-Pb-Zn deposit, electrical resistivity data reveals five mineralized zones (A, B, C, D, and E in Figure 3b), characterized by resistivity values below 510 Ωm . These mineralized zones have different geometries, sizes, and extensions. The resistivity values (mostly less than 90 Ωm) indicate that zone A has the highest enrichment in sulfides and iron oxides. Some areas of zones B and E also have higher mineralization concentrations, according to the decrease in the resistivity values in both zones [8]. The fractures and faults are identified by low-resistivity values [26–28] and reveal a structural control on the mineralization, which is characteristic of magmatic-type Ag-Pb-Zn deposits [15]. In the Minerva mineralized zone, such structures cut the profile in a NE-SW direction, like the reported direction in faults near the mine [16].

The interpretation of the ERT model in the MVT Ag-Pb-Zn deposit reveals six mineralized zones (A, B, C, D, E, and F in Figure 4b) characterized by resistivity values between 200 and 8000 Ωm . These zones have different geometries, sizes, and extensions. This interpretation also shows a highly tectonized mineral deposit and an apparent relationship between the mineralization and tectonic deformation through faults. These structures conditioned the distribution and characteristics of the mineral bodies. The identified faults

cut the profile in a NE-SW direction, coinciding with the direction of the principal faults reported in the mining district [17]. The mineralized zones A and particularly zone F can be more mineralized, because of their lower resistivities compared the other four zones. The resistivity values also indicate that in zone A, the mineral enrichment is the largest and it occurs in the north of the mining activity.

In the MVT fluorite deposit, eight mineralized zones (A, B, C, D, E, F, G, H and I in Figure 6b) were delimited with relatively moderate resistivity values (less than 5000 Ωm). These zones have different geometries, sizes, and extensions. Lower-resistivity values in zones C, G, H, and I indicate a higher amount of iron sulfides and clays in the fluorite mineralized zones. Values higher than 10,000 Ωm must be related to very compact limestone and less mineralization.

In the magmatic-type fluorite deposit, four mineralized zones (A, B, C, and D in Figure 8b) were delimited with resistivity values ranging between 180 and 1600 Ωm . In this deposit, the interpreted ERT model shows the structural control of the mineralization, and that iron oxides and clay contents are filling some fractures, as reported by Bernales-Azúcar et al. [20] in previous research. The fractures have relatively low resistivity values [6,26–28]. The interpreted ERT model also evidences the dipping direction of the limestone sequence. The faults or fractures suggested in the interpretation may be related to some faults with NE-SW directions, reported in the surroundings of the studied area [20].

In the MVT barite deposit, four mineralized zones (A, B, C, and D in Figure 9b) were delimited, with resistivity values less than 650 Ωm . These resistivity values confirm the resistivity ranges reported in other barite deposits, for example, the resistivity from 300 to 500 Ωm reported by Dakir et al. [9]. The lower-resistivity values indicate higher iron sulfides and clay contents in barite mineralization. Zones C and D have higher contents of these minerals (Figure 9b).

The location, geometry, extension, and dip of the mineralized zones of fluorite (profile 3), barite (profile 5), and Ag-Pb-Zn (profile 2), evidence their stratabound origin and, therefore, the type of mineral deposit, classified as MVT. Similarly, the location and geometry of the mineralized zones in profiles 1 and 4 show the magmatic-type fluorite and Ag-Pb-Zn deposits, respectively. The detected fractures and faults in the ERT models, as well as the heterogeneous patterns and trends defined by the mineralized zones, suggest that the mineralization is structurally controlled.

6. Conclusions

Five ERT models have been obtained on MVT-type and magmatic mineral deposits of northeastern Mexico. The geoelectrical profile allowed for the characterization of these mineral deposits and evidenced the magmatic origin of one Ag-Pb-Zn and another fluorite deposit. Similarly, the stratabound origin (MVT) of other Ag-Pb-Zn, fluorite, and barite deposits were evidenced. The interpretation allowed us to estimate the location, geometry, extension, and dip of the mineralized zones. In all 2D models, the continuity in the subsurface of the mineralization observed on the surface or mining workings was established. New mineralized zones were also revealed. The mineralized zones with moderate to low-resistivity values are related to mineral bodies with the highest Ag-Pb-Zn contents, and the fluorite and barite mineralized zones are more enriched in iron sulfides and clays. In most of the studied profiles, the structural control of the mineralization is shown, according to the identified fractures and faults. The results of this research could be used as a guide for the future of explorations of mineral deposits in this region or elsewhere.

Author Contributions: Conceptualization, J.A.B.-R. and M.A.P.-F.; methodology, M.A.P.-F.; software, J.A.B.-R.; validation, J.A.B.-R. and M.A.P.-F.; formal analysis, M.A.P.-F.; investigation, J.A.B.-R. and M.A.P.-F.; resources, J.A.B.-R.; data curation, J.A.B.-R. and M.A.P.-F.; writing—original draft preparation, J.A.B.-R.; writing—review and editing, M.A.P.-F.; visualization, J.A.B.-R.; supervision, M.A.P.-F.; project administration, J.A.B.-R.; funding acquisition, J.A.B.-R. All authors have read and agreed to the published version of the manuscript.

Funding: This research received no external funding.

Acknowledgments: We thank the Autonomous University of Coahuila and particularly the Higher School of Engineering for their support of this research.

Conflicts of Interest: The authors declare no conflict of interest.

References

1. Camprubí, A. Major metallogenic provinces and epochs of Mexico. *SGA News* **2009**, *25*, 1–20.
2. González-Sánchez, F.; Puente-Solís, R.; González-Partida, E.; Camprubí, A. Estratigrafía del Noreste de México y su relación con los yacimientos estratoligados de fluorita, barita, celestina y Zn-Pb. *Bol. Soc. Geol. Mex.* **2007**, *59*, 43–62. [[CrossRef](#)]
3. Camprubí, A.; González-Partida, E.; Richard, A.; Boiron, M.-C.; González-Ruiz, L.E.; Aguilar-Ramírez, C.F.; Fuentes-Guzmán, E.; González-Ruiz, D.; Legouix, C. MVT-like fluorite deposits and oligocene magmatic-hydrothermal fluorite–Be–U–Mo–P–V overprints in northern Coahuila, Mexico. *Minerals* **2019**, *9*, 58. [[CrossRef](#)]
4. González-Sánchez, F.; Camprubí, A.; González-Partida, E.; Puente-Solís, R.; Canet, C.; Centeno-García, E.; Atudorei, V. Regional stratigraphy and distribution of epigenetic stratabound celestine, fluorite, barite and Pb–Zn deposits in the MVT province of northeastern Mexico. *Miner. Depos.* **2009**, *44*, 343–361. [[CrossRef](#)]
5. Ford, K.; Keating, P.; Thomas, M.D. Overview of geophysical signatures associated with Canadian ore deposits. In *Mineral Deposits of Canada: A Synthesis of Major Deposit Types, District Metallogeny, the Evolution of Geological Provinces, and Exploration Methods*; Goodfellow, W.D., Ed.; Geological Association of Canada, Mineral Deposits Division: St. John's, NL, Canada, 2007; pp. 939–970.
6. Bishop, J.R.; Emerson, D.W. Geophysical properties of zinc-bearing deposits. *Aust. J. Earth Sci.* **1999**, *46*, 311–328. [[CrossRef](#)]
7. Evrard, M.; Dumont, G.; Hermans, T.; Chouteau, M.; Francis, O.; Pirard, E.; Nguyen, F. Geophysical investigation of the Pb–Zn deposit of Lontzen–Poppelsberg, Belgium. *Minerals* **2018**, *8*, 233. [[CrossRef](#)]
8. Côrtes, A.R.P.; Moreira, C.A.; Veloso, D.I.K.; Vieira, L.B.; Bergonzoni, F.A. Geoelectrical prospecting for a copper-sulfide mineralization in the Camaquã sedimentary basin, Southern Brazil. *Geophys. Int.* **2016**, *55*, 165–174. [[CrossRef](#)]
9. Dakir, I.; Benamara, A.; Aassoumi, H.; Ouallali, A.; Ait, Y. Contribution of geophysics to the study of barite mineralization in the paleozoic formations of Asdaf Tinejdad (Eastern Anti Atlas Morocco). *Econ. Environ. Geol.* **2020**, *53*, 259–269. [[CrossRef](#)]
10. Akpan, A.E.; Ebong, E.D.; Ekwok, S.E.; Joseph, S. Geophysical and geological studies of the spread and industrial quality of Okurike barite deposit. *Am. J. Environ. Sci.* **2014**, *10*, 566–574. [[CrossRef](#)]
11. Jochymczyk, K.; Cabala, J.; Poreba, A. Application of resistivity imaging to recognition of geological structure in the area of shallow Zn-Pb ore bodies (preliminary study). *Acta Geodyn. Geomater.* **2006**, *3*, 131–138.
12. Tritlla, J.; Canals, A. Mineralizaciones Estratoligadas de Metales de Base en Carbonatos, Rocas Siliciclásticas. In *Atlas de Asociaciones Minerales en Lámina Delgada*; Melgarejo, J.C., Ed.; Edicions de la Universitat de Barcelona: Barcelona, Spain, 1997; pp. 273–286.
13. Tritlla, J.; Levresse, G.; Corona-Esquivel, R.; Banks, D.; Lamadrid, H.; Bourdet, J. Depósitos de Pb-Zn-Cu-Ba-F-Sr epigenéticos estratoligados en series sedimentarias en relación con salmueras de cuenca: Depósitos de tipo “Mississippi Valley” (MVT) y similares en México. *Bol. Soc. Geol. Mex.* **2006**, *58*, 103–139. [[CrossRef](#)]
14. Camprubí, A. Tectonic and metallogenic history of Mexico. In *Tectonics, Metallogeny, and Discovery: The North American Cordillera and Similar Accretionary Settings*; Colpron, M., Bissig, T., Rusk, B.G., Thompson, J.F.H., Eds.; Society of Economic Geologists: Littleton, CO, USA, 2013; Volume 17, pp. 201–243.
15. Megaw, P.K.M.; Ruiz, J.; Titley, S.R. High-temperature, carbonate-hosted Ag-Pb-Zn(Cu) deposits of northern Mexico. *Econ. Geol.* **1988**, *83*, 1856–1885. [[CrossRef](#)]
16. Herrera-Monreal, J.C.; Rodríguez-Rodríguez, J.S. *Carta Geológico-Minera Las Eutimias H13-D77, Coahuila, Escala 1: 50,000*; Servicio Geológico Mexicano: Pachuca de Soto, Mexico, 2006.
17. Montañez-Castro, A. *Carta Geológico-Minera San José de Raíces G14-C66, Escala 1: 50,000*; Servicio Geológico Mexicano: Pachuca de Soto, Mexico, 2007.
18. Santiago-Carrasco, B.; Maciel-Hernández, M.A. *Carta Geológico-Minera Sabanilla G14-C41, Coahuila y Zacatecas, Escala 1: 50,000*; Servicio Geológico Mexicano: Pachuca de Soto, Mexico, 2007.
19. Ramírez-Gutiérrez, J.G.; Chávez-Rangel, F.J. *Carta Geológico-Minera Jaboncillos H13-D57, Coahuila, Escala 1: 50,000*; Servicio Geológico Mexicano: Pachuca de Soto, Mexico, 2006.
20. Bernales-Azúcar, J.M.; Camacho, J.M.; Luna-Castillo, V.M. *Carta Geológico-Minera Mariano Escobedo, Coahuila, Escala 1: 50,000*; Servicio Geológico Mexicano: Pachuca de Soto, Mexico, 2013.
21. *Manual de Instrucciones para SuperSting TM con Sistema de Resistividad Automática SwiftTM y PI*; Version 01.01.38, SuperSting R1/PI; Advanced Geosciences, Inc (AGI): Austin, TX, USA, 2006.
22. Dahlin, T.; Zhou, B. A numerical comparison of 2D resistivity imaging with 10 electrode arrays. *Geophys. Prospect.* **2004**, *52*, 379–398. [[CrossRef](#)]
23. Okpoli, C.C. Sensitivity and Resolution Capacity of Electrode Configurations. *Int. J. Geophys.* **2013**, *2013*, 1–12. [[CrossRef](#)]

24. Villela-Y-Mendoza, A.; Perez-Flores, M.A.; Ochoa-Tinajero, L.E.; Vargas-Huitzil, E. Applying resistivity (dipole-dipole, Schlumberger, and Wenner) joint inversion to detect endokarst features in Quintana Roo, México. *J. S. Am. Earth Sci.* **2021**, *106*, 103041. [[CrossRef](#)]
25. *Instruction Manual for EarthImager*, Version 2.4.0; Resistivity and IP Inversion Software; Advanced Geosciences, Inc (AGI): Austin, TX, USA, 2009.
26. Park, J.-O.; You, Y.-J.; Kim, H.J. Electrical resistivity surveys for gold-bearing veins in the Yongjang mine, Korea. *J. Geophys. Eng.* **2009**, *6*, 73–81. [[CrossRef](#)]
27. Gómez-Ortiz, D.; Fernandezremolar, D.C.; Granda, Á.; Quesada, C.; Granda, T.; Prieto-Ballesteros, O.; Molina, A.; Amils, R. Identification of the subsurface sulfide bodies responsible for acidity in Río Tinto source water, Spain. *Earth Planet. Sci. Lett.* **2014**, *391*, 36–41. [[CrossRef](#)]
28. Bran, D.M.; Tassone, A.A.; Menichetti, M.; Cerredo, M.E.; Lozano, J.G.; Lodolo, E.; Vilas, J.F. Shallow architecture of Fuegian Andes lineaments based on Electrical Resistivity Tomography (ERT). Evidences of transverse extensional faulting in the central Beagle Channel area. *Andean Geol.* **2018**, *45*, 1–34. [[CrossRef](#)]